Friedrich-Alexander-Universität Erlangen-Nürnberg

Faculty of Engineering
Department of Chemical and Biological Engineering
Institute for Multiscale Simulation

A Tool to Analyze Random Packings of Meissner Tetrahedra

Bachelor's thesis
Frederik Keil

written under the supervision of
Dr. Achim Sack

Erlangen, 10.08.2023

Contents

List of Figures

1. Introduction

One usually comes across packings in the supermarket in the form of pyramidal stacked oranges or translucent cylinders filled with candies. While many properties of sphere packings are known [1], the packing properties of Meissner tetrahedra are jet unknown.
Meissner tetrahedra are convex bodies of constant width, similar to spheres. This means that if clamped between two parallel planes touching the surface, the distance between them is always constant and known as diameter.[2]
Other than spheres Meissner tetrahedra have an orientation in three dimensional space that stems from their construction [3]. This means that besides the diameter and location of the center, three Euler angles are needed to fully describe the Meissner tetrahedra in three dimensional space [4].
X-ray tomography is a non-destructive method for visualising the internal structure of an object [5].
In this thesis X-ray tomography is used to study the packing properties of Meissner tetrahedra within a cylindrical container from tomographic data. Therefore an algorithm is developed to obtain the packing density, the position and the orientation of the individual Meissner tetrahedra within a lose packing.

2. Theory

2.1 Construction of Meissner tetrahedra

There are two non congruent Meissner tetrahedra, which are both based on a regular tetrahedron of side length s as shown in Fig.2.1a [6].
The regular tetrahedron is first transformed in a Reuleaux tetrahedron. This is done by placing one sphere with its center on each of the four vertices of the regular tetrahedron. The radius of these spheres must be equal to the side length of the regular tetrahedron. This condition forces the spheres to intersect, as shown in Fig.2.1b. The intersection of all of the four spheres is called Reuleaux tetrahedron. Fig.2.1c shows the Reuleaux tetrahedron from top view and Fig.2.1d from side view. A Reuleaux tetrahedron is yet not a solid of constant width, the distance between the midpoints of two opposite edges, $\left(\sqrt{3}-\sqrt{2}/2\right)s \approx 1.0249s$ is slightly larger than the distance s between a vertex and a spherical face or two vertices.[3], [6]–[8]
The Reuleaux tetrahedron can be transformed in a Meissner tetrahedron by replacing three of the six sharp edges with three round edges, which can be done in two ways: Either the three round edges meet in one vertex of the Reuleaux tetrahedron creating Meissner tetrahedron M_V or the three round edges enclose one face of the Reuleaux tetrahedron creating Meissner tetrahedron M_F. Fig.2.2c shows M_V from top view and Fig.2.2d shows M_V from side view. Fig.2.2g shows M_F from bottom view and Fig.2.2h shows M_F from side view. The round edges are produced by intersecting a regular tetrahedron placed with its edge on the edge of the underlying tetrahedron of the Reuleaux tetrahedron as shown in Fig.2.2a and Fig.2.2e. The circular edge of the Reuleaux tetrahedron creates an intersections with the straight edges of the regular tetrahedron and is removed. The resulting circular segment is rotated around the straight edge of the tetrahedron creating a spindle torus as shown in Fig.2.2b and Fig.2.2f. The rounded edges correct the small mismatch in diameter resulting in a Meissner tetrahedron with the property of being of constant width s, which is the edge length of the tetrahedron from the

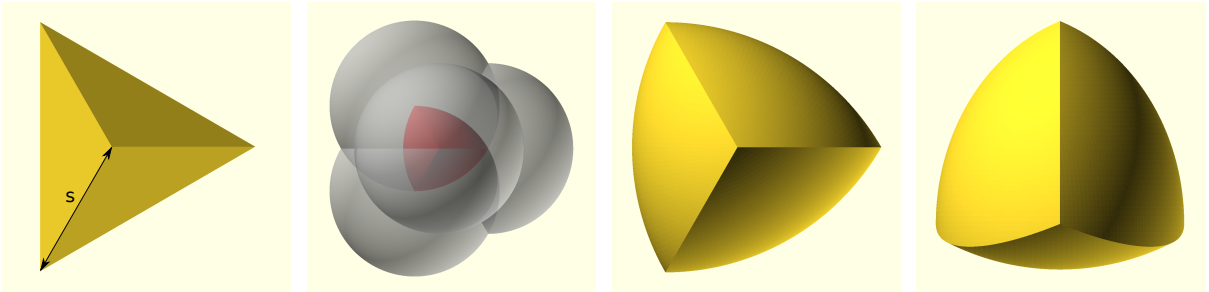

(a) Regular tetrahedron (top view) (b) Intersection of spheres (top view) (c) Reuleaux tetrahedron (top view) (d) Reuleaux tetrahedron (side view)

Figure 2.1: Construction of a Reuleaux tetrahedron

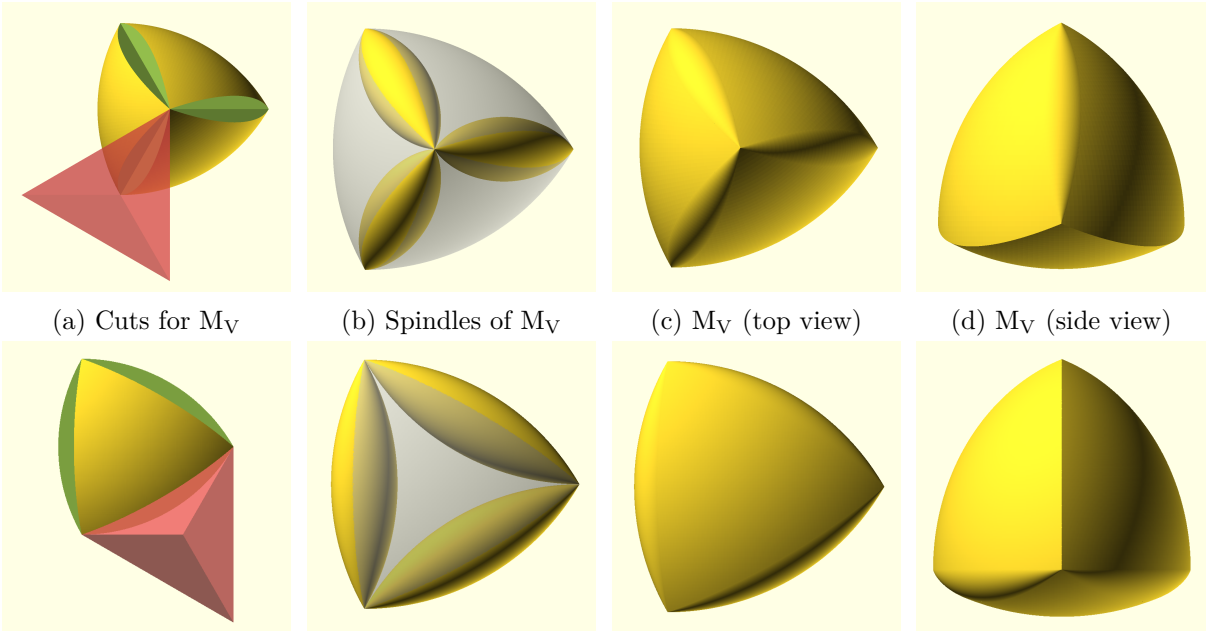

(a) Cuts for M_V (b) Spindles of M_V (c) M_V (top view) (d) M_V (side view)

(e) Cuts for M_F (f) Spindles of M_F (g) M_F (bottom view) (h) M_F (side view)

Figure 2.2: Construction of the two Meissner tetrahedra M_V and M_F

beginning.[3], [6]–[8]

2.2 Properties of Meissner tetrahedra

M_V and M_F have identical volume and surface area. They consist both of four vertices, four spherical surfaces, three toroidal surfaces or rather round edges and three circular arcs as sharp edges in both cases. One of the four vertices is unique. In case of M_V there is one vertex where the three spindle tori meet and in case of M_F there is one vertex where three circular arcs meet. This vertex gives the Meissner tetrahedra an orientation in three dimensional space and is therefore called directing vertex. The other vertices are called ordinary vertices. Around the axis through the centroid and the directing vertex, the Meissner tetrahedra have a threefold rotational symmetry. The centroid of a Meissner tetrahedron characterizes its position in three dimensional space. The orientation of a Meissner tetrahedron can be characterized by three Euler angles. Two Euler angles characterize the direction in which the directing vertex points and the third Euler angle characterize the rotation around the axis through the centroid and the directing vertex.[3], [6]

2.3 Packing density and tomography

The packing density of a regular packing is defined as the volume fraction of a unit cell [9]. The densest regular sphere packings have a packing density of 0.74 [10], Reuleaux tetrahedra have a value of 0.79 [11] and regular tetrahedra 0.85 [12].
The packing density of a random packing can be calculated locally as fraction of the particle volume to the volume of its Voronoi cell or globally as fraction of the total particle volume in some space V_{occupied} to the volume of the space itself V_{total} [13]–[15]. For example is the packing density of random monodisperse sphere packings found to be in between 0.562 (lose packings)

and 0.64 (dense packings) [16]. The densest packing of random packings of tetrahedral dice is 0.76 [17].
With X-ray tomography, two dimensional shadow projects of an three dimensional object under different angles are obtained and converted into a three dimensional reconstruction of this object. This reconstruction represents the object on an equally spaced three dimensional lattice or 3D array. One cube of this three dimensional lattice is called voxel and contains a grey-scale value which is equal to the local X-ray absorption. The number of voxels per volume depends on the resolution of the computer tomographic scan.[5], [18], [19]
In a computer tomographic scan the number of voxels which approximate the real shape of an object is proportional to the volume of that object [20]. Therefore, the global packing density Φ can be calculated as the ratio of the number of occupied voxels or rather object voxels in some space and the total number of voxels of this space, Eq.(2.1).

$$\Phi = \frac{V_{\text{occupied}}}{V_{\text{total}}} \rightarrow \frac{N_{\text{occupied}}}{N_{\text{total}}} \tag{2.1}$$

3. Code development

In the following section, the method how to obtain the packing density, the position and the orientation of the Meissner tetrahedra within a packing from tomographic data will be explained. The method is developed for a packing within a cylindrical container. The longitudinal direction of this cylinder or packing is defined as z-axis. Planes that are perpendicular to the z-axis are called layers or slices.

3.1 Packing density

A cylindrical region of interest Fig.3.1c is first defined with a total volume V_{total} containing N_{total} voxels. This is done by placing a circular mask as shown in Fig.3.1b on every grayscale slice of the three dimensional array along the z-axis like in Fig.3.1a. The radius is chosen such that the circular shape of the container wall is removed. The height of the region of interest is chosen so that the bottom of the container is removed.
To access the number of occupied voxels N_{occupied}, it must be distinguished between voxels that belong to Meissner tetrahedra or to surrounding air. This is done by using grey-value based image segmentation. Voxels that belong to Meissner tetrahedra have a higher absorbance and appear brighter on a grayscale image than voxels that belong to surrounding air. Therefore every pixel that is brighter than a certain threshold belongs to a Meissner tetrahedron and is set to one. Every pixel darker than that threshold belongs to surrounding air and is set to zero. Instead of generating a different threshold for every layer of the 3D array, one global threshold is generated by OTSU's method for the entire volume. This way the result is more robust towards image noise. OTSU's method assumes a bimodal grey-value distribution and finds a threshold that divides it into two classes.[21]
The result is a binary image in which occupied voxels have a value of one and background voxels a value of zero. Fig.3.1d shows a binary slice of the packing. Occupied or rather object voxels appear white, while unoccupied voxels that belong to air appear black.
Instead of directly calculating the global packing density Φ, a layer based packing density ϕ_i which depends on the height is first calculated. The global packing density Φ is then calculated as the average of the layer based packing densities, as shown in Eq.(3.1).

$$\Phi = \frac{N_{\text{occupied}}}{N_{\text{total}}} = \frac{\sum N_{i,\text{occupied}}}{N_{\text{total}}} = \frac{\sum \frac{N_{i,\text{occupied}}}{N_{i,\text{total}}}}{\frac{N_{\text{total}}}{N_{i,\text{total}}}} = \frac{\sum \phi_i}{N_{\text{slice}}} \tag{3.1}$$

3.2 Position

To access the position of the individual objects, region based segmentation is used. To do so, the container wall and bottom is removed by applying a circular mask on every slice of grey scale

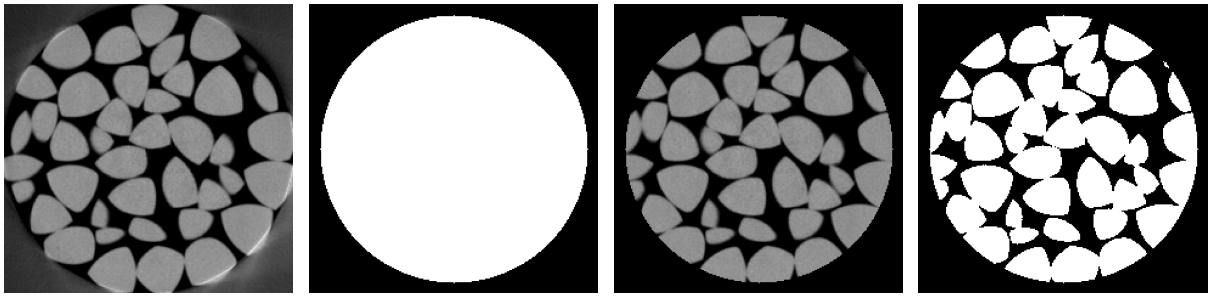

(a) Greyscale image (b) Mask (c) Masked image (d) Binarized image

Figure 3.1: From grayscale image to binary image

array before using OTSU's method for binarization as in part 3.1. Fig.3.2a shows a masked grey scale slice.
The mask is need because the container wall and bottom has a similar X-ray absorption as the 3D-printed Meissner tetrahedra leading to a similar grey value. Therefore, OTSU's method can't distinguish between voxels that belong to the contain walls or bottom and voxels that belong to Meissner tetrahedra.
The circular mask removes also parts of the Meissner tetrahedra. Those partly cut Meissner tetrahedra are filtered out once their position is known.
Sometimes small voids appear inside the Meissner tetrahedra. This can happen due to image noise or bad pixels on the detector. Those voids are removed by applying the connected-components-3d algorithm on the inverted image. The algorithm labels voxels that belong to the same cluster of voxels with the same value [22]. Since the air around the objects forms one big cluster, all smaller clusters must belong to voids inside the objects and can therefore be removed [15]. Fig.3.2b shows the binarized image of the previous slice.
To separate the individual Meissner tetrahedra, the Euclidean Distance Transform of the binary volume is calculated. Object voxels are labeled according to their Euclidean Distance to the nearest background voxel [23]. Fig.3.2c shows the Euclidean Distance transform of the same slice. A brighter color corresponds to a higher value and therefore a greater distance to the background.
The Euclidean Distance Transform is binarized using a manually chosen threshold so that only the voxels close to the centroids of the Meissner tetrahedra remain, as shown in Fig.3.2d. If the threshold is larger than the highest value of the Euclidean Distance Transform, all objects are fully eroded. If chosen too small, the objects are not fully separated.[15]
By using the connected-components-3d algorithm voxels that belong to same core are labeled with the same value. Fig.3.2e shows the labeled cores. Different colors correspond to different labels and therefore different Meissner tetrahedra. At this point, the label with the highest value is equal to the number of Meissner tetrahedra contained in the packing [22].
By applying the watershed-ift algorithm, the boundaries between the individual Meissner tetrahedra are found [23]. Fig.3.2f shows the separated Meissner tetrahedra that appeared as one white structure in 3.2b.
The position of the Meissner tetrahedra is defined as the centroid of each Meissner tetrahedron and is described by its three components X_j, Y_j and Z_j. Every component of the centroid is defined as the average value of all x-, y- and z-components of voxels belonging to one Meissner tetrahedron, Eq.(3.2).[24]

$$X_j = \frac{\sum x_{j,i}}{N},\ Y_j = \frac{\sum y_{j,i}}{N},\ Z_j = \frac{\sum z_{j,i}}{N} \tag{3.2}$$

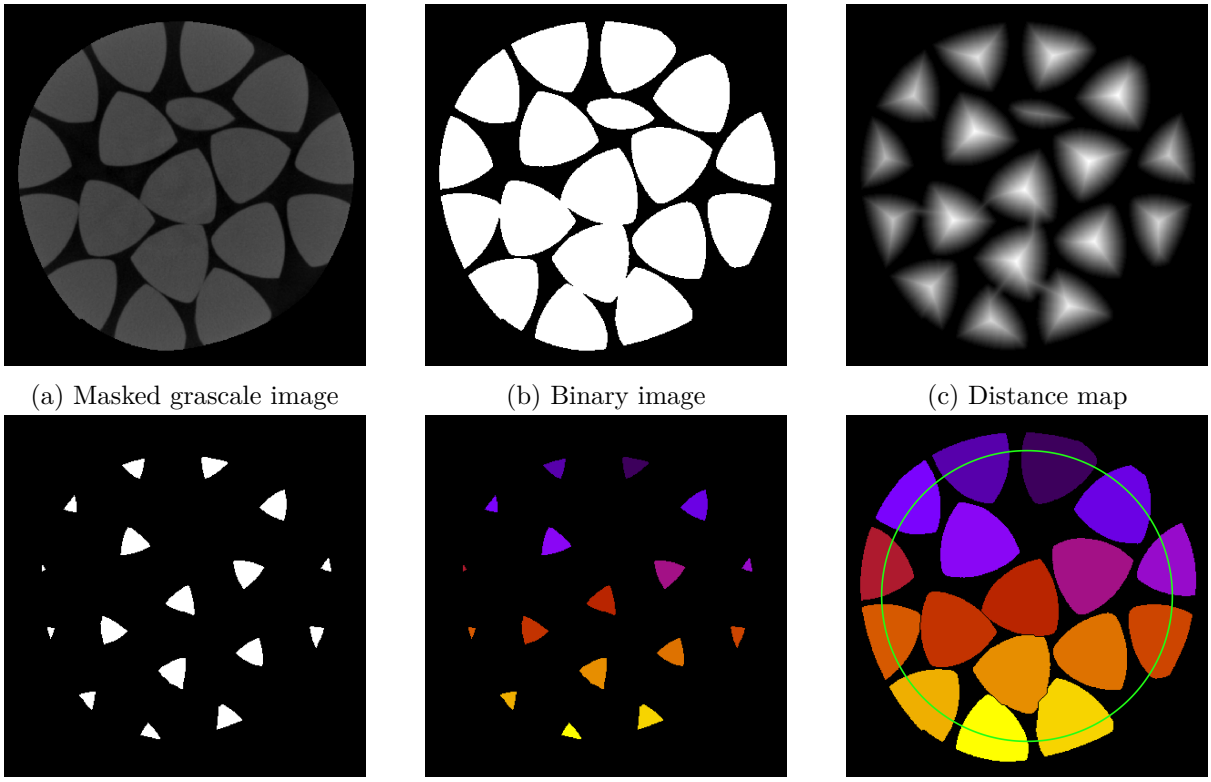

(a) Masked grascale image (b) Binary image (c) Distance map

(d) Separated cores (e) Labeled cores (f) 3D Watershed

Figure 3.2: Separation of Meissner tetrahedra

The centroid is not equal to the center of the tetrahedron the Meissner tetrahedra are based on. The small shift due to the shape of the surface of the Meissner tetrahedra is neglected.
The centroids are used as filter criterion to remove Meissner tetrahedra that are touching the wall or bottom of the container and might have been cut by the circular mask, when removing the container wall and bottom. Meissner tetrahedra exceeding the radius of the region of interest as shown in Fig.3.2f or the depth of the region of interest are removed.[15]

3.3 Orientation

To obtain the orientation of the Meissner tetrahedra within the region of interest the vertices of the Meissner tetrahedron need to be found. Vertices of a regular object like a tetrahedron have the property that the distance between the centroid and a vertex is maximal [25]. This property is used to find the vertices of the Meissner tetrahedra.
To isolate the vertices, first a sphere is placed on the centroid of each Meissner tetrahedra. The radius of the sphere has a value in between the radius of the inscribed and circumscribed sphere of the tetrahedron the Meissner body is based on. This sphere is then subtracted from the Meissner tetrahedron by setting all object voxels to zero whose distance to the centroid is smaller than the radius of the sphere, which separates the groups of voxels close to the vertices of the Meissner tetrahedra. Due to image noise, these voxel groups must be filtered according to their size to ensure that only the four largest remain.
Within every voxel group, the voxel V_i with the largest distance to the centroid C is selected as

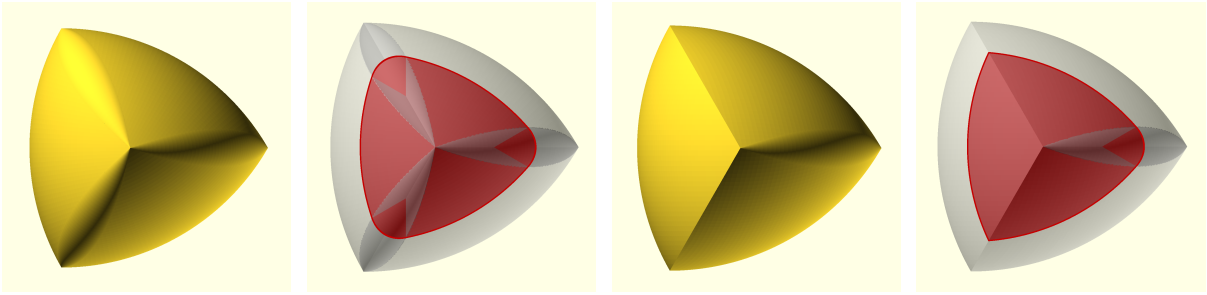

(a) Directing vertex (b) Intersection (c) Ordinary vertex (d) Intersection

Figure 3.3: Difference between a directing vertex and an ordinary vertex

vertex, Eq.(3.3).

$$\max_i \quad |\overrightarrow{CV_i}| \tag{3.3}$$

Now that the vertices are known it must be differentiated between a directing vertex and an ordinary vertex. For each vertex a intersecting plane is constructed with a normal vector pointing from the vertex to the centroid, parallel to $\overrightarrow{CV_i}$. The area contained in this intersecting plane depends on the type of vertex.
For Meissner tetrahedron $\mathrm{M_V}$ the plane with a normal vector pointing from a directing vertex to the centroid contains a smaller area than a plane with a normal vector pointing from an ordinary vertex. For Meissner tetrahedron $\mathrm{M_F}$ would it be the other way around.
Fig.3.3 shows the intersection area for $\mathrm{M_V}$ from a directing vertex Fig.3.3b and from an ordinary vertex Fig.3.3d in the same distance from the vertex. The three rounded edges in case of a directing vertex make the intersection area smaller. The difference between the two areas can be calculated according to Eq.(3.4).

$$\epsilon = \left| \frac{A_{\text{ordinary}} - A_{\text{directing}}}{A_{\text{ordinary}}} \right| \tag{3.4}$$

Fig.3.4 shows the difference in percent between the intersection plane from a directing and an ordinary vertex along the height h_p of Meissner tetrahedron $\mathrm{M_V}$. The difference increases from the basis towards the vertex but is in general rather small, ranging from 0 % to 3 %.
In order to make the detection of the directing vertex as reliable as possible, several planes above $0.6 \cdot h_p$ are used. The directing vertex of $\mathrm{M_V}$ is the one vertex creating the most planes with the smallest intersection areas.
Once all vertices are known and classified the orientation can be calculated. First the vector $\overrightarrow{CV_D}$ pointing from the centroid to the directing vertex is defined. The azimutahl angel φ is then defined as the angle between the projection of $\overrightarrow{CV_D}$ in the x-y-plane and the x-axis ranging from zero to 2π. The polar angel θ is defined as the angle between $\overrightarrow{CV_D}$ and the z-axis ranging from zero to π.
Knowing the azimuthal φ and polar θ angle the Meissner tetrahedron can be rotated into an upright position where the directing vertex is on the positive side of z-axis. The rotation angle γ characterizes the rotation of the Meissner tetrahedron around $\overrightarrow{CV_D}$. Since the Meissner tetrahedron is now in an upright position the ordinary vertices are projected into the x-y-plane. The rotation angle γ is defined as the angle between the projected vertex in the first or fourth quadrant and the y-axis. Meissner tetrahedra have a threefold rotational symmetry [3] which is why the rotation angel γ ranges from 0 to $2\pi/3$.
Fig.3.5 summarizes the described algorithm. Once the Meissner tetrahedra are isolated from

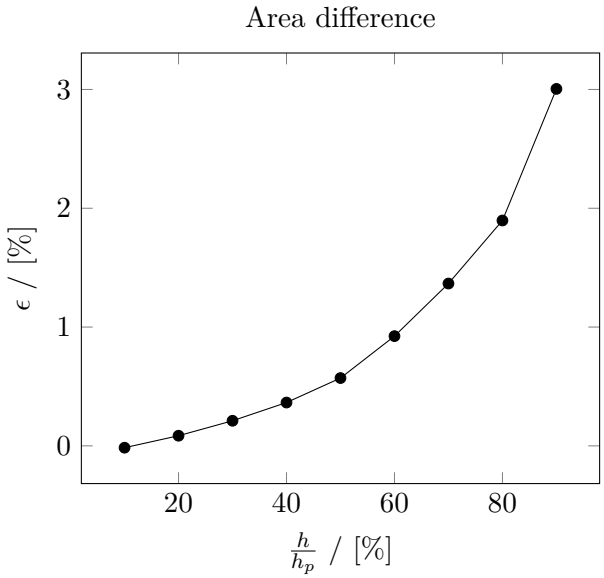

Figure 3.4: Area difference between a directing and an ordinary vertex along the height

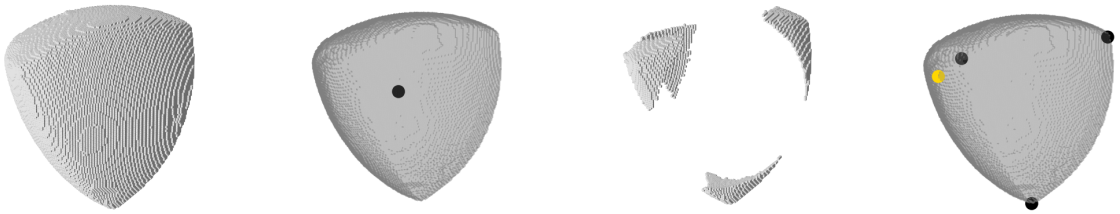

(a) Isolated M_V (b) Centroid (c) Subtraction (d) Vertices

Figure 3.5: Key steps of the algorithm

each other their centroid is calculated. Fig.3.5a shows an isolated Meissner tetrahedron. The centroid is shown in Fig.3.5b as a black dot. At the centroid a sphere is placed and subtracted from the Meissner tetrahedra, revealing the vertex candidates shown in Fig.3.5c. Based on the vertex candidates and the area difference the vertices are determined. Fig.3.5d shows the directing vertex as a yellow dot and the three ordinary vertices as black dots for the angle calculation.

4. Experimental setup

In this section the manufacturing process of the Meissner tetrahedra and the image acquisition will be explained.

4.1 Preparing the packings

Since booth Meissner tetrahedra have equal volume and surface area we randomly choose M_V, three round edges combined in one vertex for investigation.[3]
The Meissner tetrahedra were produced by a stereo lithography based 3D-printer from resin. The needed support structure for 3D-printing creates small marks on the surface which were ground off. Afterwards the yet soft Meissner tetrahedra are cured under UV light for hardening. The hardening process causes warping giving the Meissner tetrahedra a slight asymmetry, meaning that the distance between the vertices varies.
A diameter s of 15 mm was chosen to ensures a noticeable difference between a sharp and round edge. The radius of curvature at a midpoint of a round edge is 2 mm. The Meissner tetrahedra have a density of $1.2\,\mathrm{g/cm^3}$.
To determine the packing density a cylindrical PMMA container with an inner diameter D of 84 mm was filled with 150 Meissner tetrahedra creating a lose monodisperse packing. The ratio of the container diameter D and the particle diameter s is $D/s = 5.6$.
To determine the location and orientation a second smaller packing counting 60 Meissner in a cylindrical container out of cardboard with a diameter D of 65 mm was used. This time the ration D/s is 4.3. Fig.4.1 shows the prepared packings.

(a) Packing of 150 Meissner tetrahedra (side view)

(b) Packing of 150 Meissner tetrahedra (top view)

(c) Packing of 60 Meissner tetrahedra (top view)

Figure 4.1: Experimental setup

4.2 Image acquisition

For the large system with 150 Meissner tetrahedra the acceleration voltage was set to 150 kV and the current to 200 μA. The exposure time was set to 250 ms. The resolution of the reconstructed volume is 341.78 μm/voxel. The reconstructed volume contains $240 \times 240 \times 100$ voxels.
For the small system with 60 Meissner tetrahedra the acceleration voltage was set to 60 kV and a the current to 500 μA. The exposure time was set again to 250 ms. The resolution of the reconstructed volume is 157.94 μm/voxel. The reconstructed volume contains $348 \times 348 \times 480$ voxels.

5. Results and discussion

5.1 Packing density

Fig.5.1 shows the dependency of the layer based or local packing density ϕ on the longitudinal position z as well as the global packing density Φ. Because of gravity acting on the packing, Meissner tetrahedra touching the base of the container are forced in an up right position with a vertex pointing upwards and a spherical face touching the bottom. The ordered Meissner tetrahedra of the packing create a higher packing density close to the bottom and a periodic trend of the packing density. With increasing height the effect of the bottom vanishes, which can be seen in the decreasing amplitude of the packing density. The global packing density Φ is equal to 0.68 and therefore in between the packing density of random loose spheres (0.56) and random dense tetrahedra (0.76) [16], [17].

5.2 Number of objects and volumes

The algorithm is able to detected all 60 Meissner tetrahedra of the packing. The region of interest contains 13 Meissner tetrahedra. The standard deviation of their volume is 0.5 % compared to the average volume of $1.376\,\mathrm{cm}^3$. Fig.5.2 shows the volume of each Meissner tetrahedra as black dots and the average value as red line.
Since there is no larger volume, for example twice the volume of one Meissner tetrahedra and the number of found Meissner tetrahedra is correct the separation must be successful.[15]

5.3 Position and orientation

Fig.5.3 shows the z-coordinates and Fig.5.4 show the x- and y- coordinates of the Meissner tetrahedra within the region of interest. The black circle in the background of Fig.5.4 represents the diameter the cylindrical container, the black dashed circle the diameter of the region of interest.
The algorithm finds 52 vertices. This is correct because each of the 13 Meissner tetrahedra has 4 vertices. The average distance between the vertices of one Meissner tetrahedron and its standard deviation are shown in Fig.5.5. The Meissner tetrahedra are based on regular tetrahedra of the same size with equally long sides. Therefore the average distance between the vertices should be equal. This can be seen in Fig.5.5. The bars have a similar height of either 14.4 mm or 14.5 mm. The largest standard deviation of the length between the vertices is 0.357 mm for the Meissner tetrahedron with the ID 2 which is 2.5 % of the average edge length of 14.4 mm.
The obtained angles are shown in Fig.5.6, Fig.5.7 and Fig.5.8. All three angles have a rather random distribution. In Fig.5.8 there is one outlier. The Meissner tetrahedron with ID 9 has an angle of $\gamma = 2.2$ which is larger than $2\pi/3 \approx 2.1$ and should therefore not be possible.
One explanation for this are the unequal distances between the vertices, creating a asymmetric

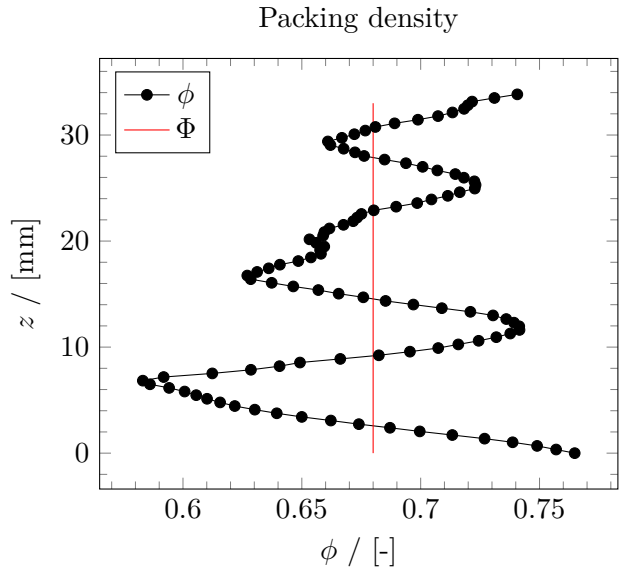

Figure 5.1: Local ϕ and global Φ packing density of a random loose packing

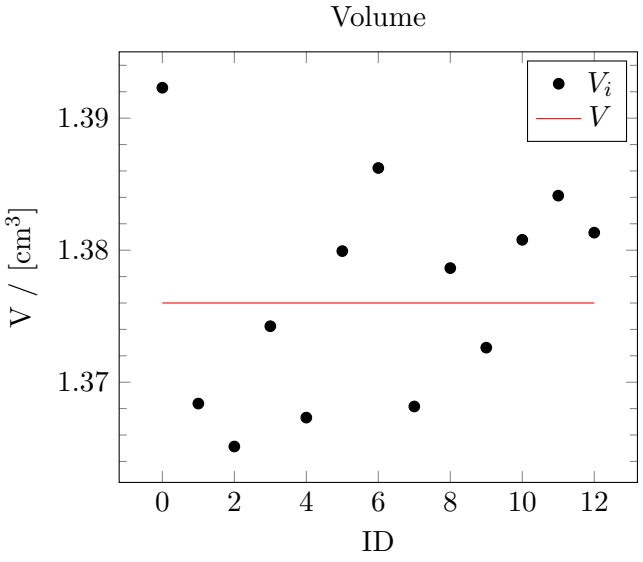

Figure 5.2: Volume of each Meissner tetrahedron

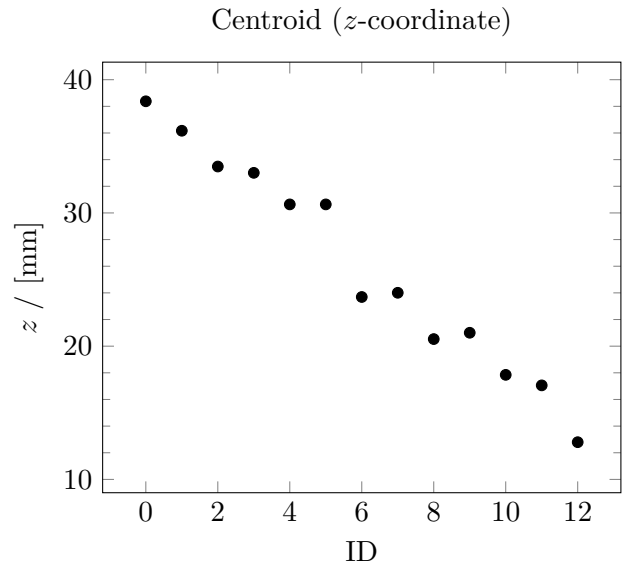

Figure 5.3: z-coordinate of the centroid of each Meissner tetrahedron

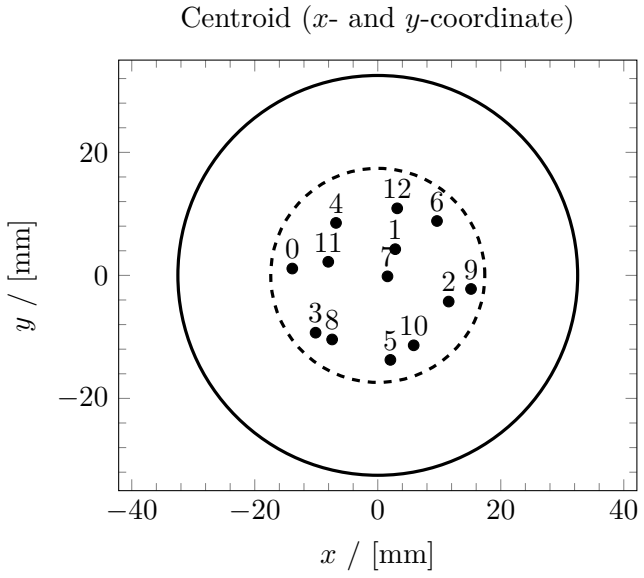

Figure 5.4: x- and y-coordinate of the centroid of each Meissner tetrahedron

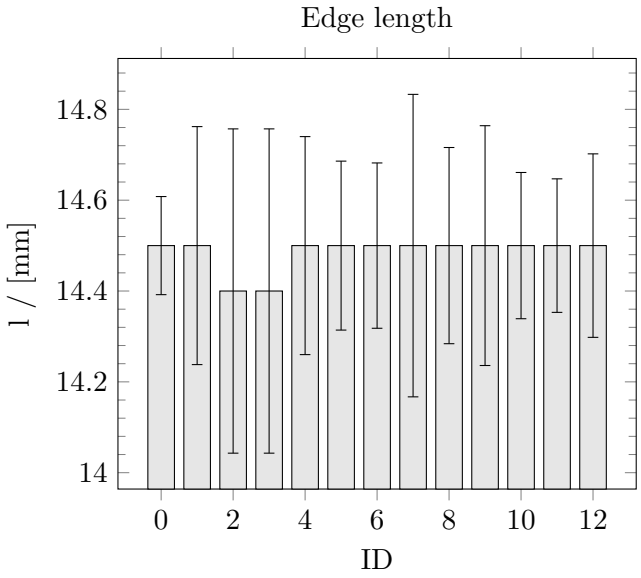

Figure 5.5: Edge length of each Meissner tetrahedron

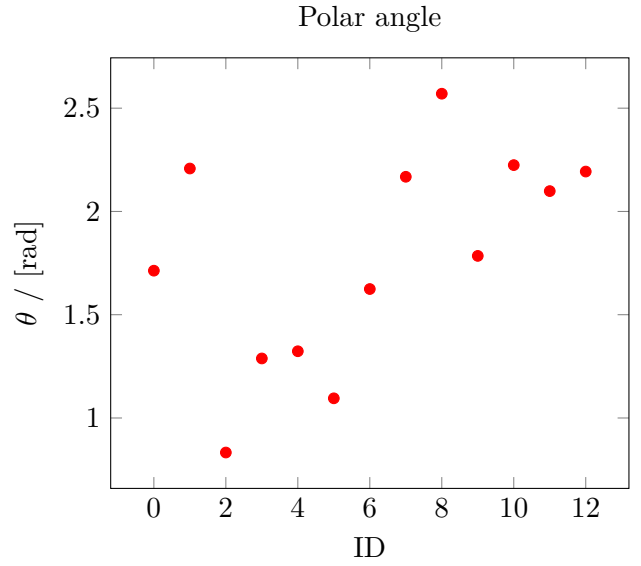

Figure 5.6: Polar angle θ in rad.

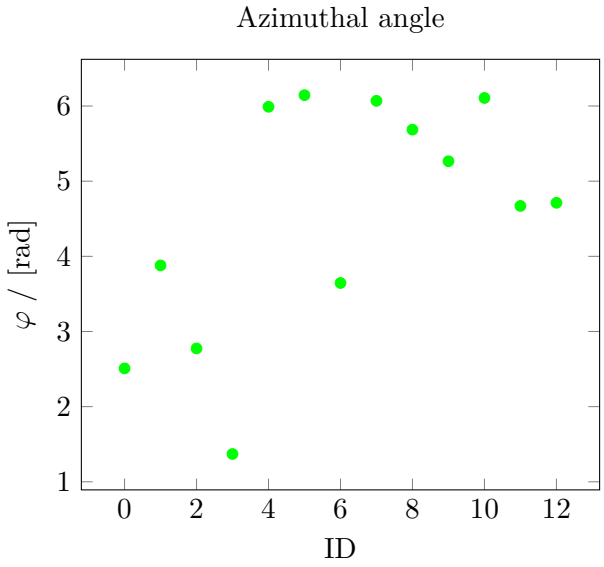

Figure 5.7: Azimuthal angle φ in rad.

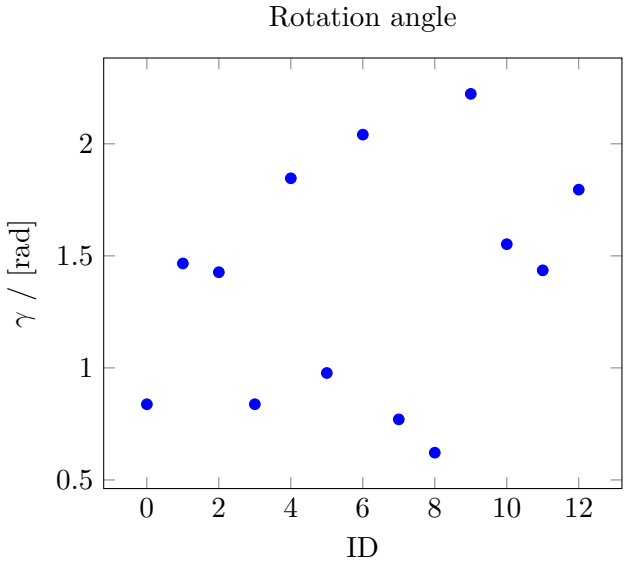

Figure 5.8: Rotation angle γ in rad.

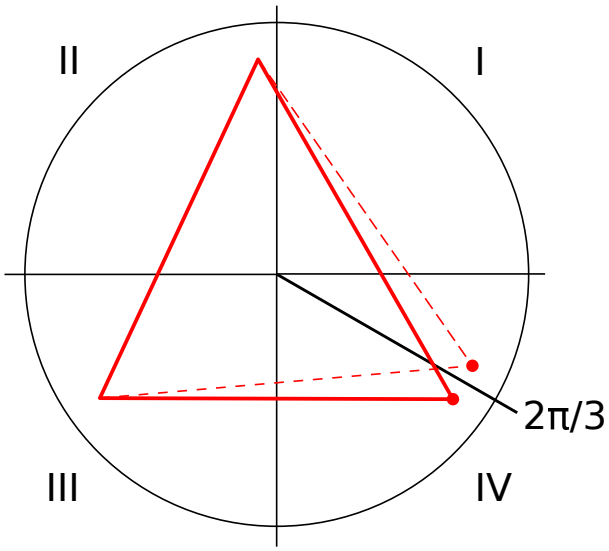

Figure 5.9: Effect of an asymmetric basis

projection of the basis in x-y-plane. Fig.5.9 shows a asymmetric basis represented by the red triangle. The dashed red triangle shows the asymmetric triangle if it was symmetric.
The algorithm first looks for a vertex in the first quadrant. If there is no vertex, there must be a vertex in the fourth quadrant at an angle smaller than $2\pi/3$ because of the threefold rotational symmetry of an equilateral triangle.
In case of the symmetric triangle this works. The vertex of the dashed symmetric triangle lies within the fourth quadrant at an angle smaller than $2\pi/3$. In case of the asymmetric red triangle the algorithm finds a vertex in the fourth quadrant but at an angle larger than $2\pi/3$.
It is possible to create a CAD model of the investigated packing in order to see weather the obtained positions and angles are plausible. There should not be for example a vertex penetrating a face of another Meissner tetrahedron. Such a configuration would indicate a wrong description of the position or orientation. Fig.5.10 shows the CAD clone as well as the CT scan for comparison. The yellow Meissner tetrahedra in Fig5.10a indicate the region of interest. From that comparison it becomes clear that the proposed method seems to work. The Meissner tetrahedra are tangential to each other and the orientation of the round edges match.

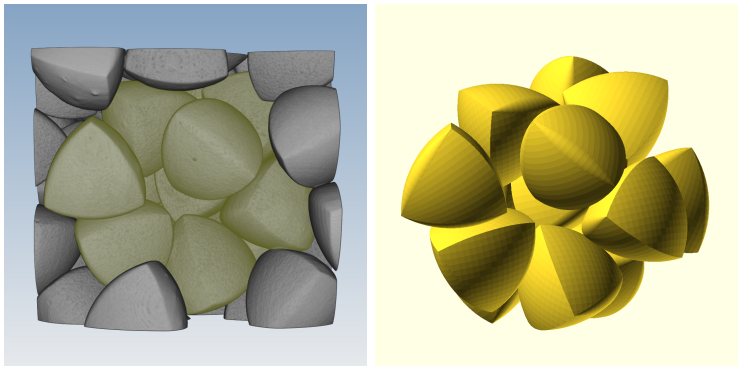

(a) CT scan (top view) (b) CAD clone (top view)

Figure 5.10: Consistency check

6. Conclusion and outlook

This thesis has shown that it is possible to obtain the packing density, the positions and the orientations of Meissner tetrahedra within a random loose packing from tomographic data. The packing density was calculated for a system with a ratio of D/s of 5.6 after the Meissner tetrahedra have been poured in the container and was found to be 0.68, Fig5.1. In order to confirm the packing density a larger container or a container with smaller Meissner tetrahedra must be invested. Neudecker et al. have used a ratio of D/s of 15 [26]. Beside of that the experiment should be repeated several times with a fixed preparation protocol to create comparable packings.
The number of Meissner tetrahedra which can be detected is limited by the need of a region of interest that separates the container wall form the Meissner tetrahedra. This reduces the number of Meissner tetrahedra from 60 to 13. In order to be able to detect Meissner tetrahedra touching the wall a container with a much lower absorption than the Meissner tetrahedra can be used. In this case the wall could be removed by OTSU's method.
The precision of the orientation is limited to the resolution of tomographic data. Scans with higher resolution would help finding the directing vertex because the curvature of the spindle surface would be resolved to a higher degree.
Since the shape of the surface of a Meissner tetrahedron is not symmetric like the shape of the surface of a Reuleaux tetrahedron or regular tetrahedron the calculated centroid is not equal to the actual center of the tetrahedron the Meissner tetrahedron is based on. This offset was neglected. The real center can be obtained by first calculating the centroid as it is done right know to find the vertices. Since the vertices are the same vertices as of the tetrahedron the Meissner tetrahedron is based on the center is the average of the vertex coordinates.
When calculating the vertices it sometimes happens that there are several voxels with the same maximal distance to the centroid. In such a case the first voxel having the maximal distance from the centroid is chosen. In order to come closer to the real vertex it would be better to average the position among the maximal distance voxels. This could reduce the standard deviation of the distance between the vertices in Fig.5.5.

Bibliography

[1] M. Leppmeier and J. M. Wills, *Kugelpackungen von Kepler bis heute: eine Einführung für Schüler, Studenten und Lehrer*, 1st ed. Vieweg, 1997.

[2] H. Martini, L. Montejano, and D. Oliveros, *Bodies of constant width*, 1st ed. Springer, 2019.

[3] B. Kawohl and C. Weber, "Meissner's mysterious bodies," *The Mathematical Intelligencer*, vol. 33, no. 3, 2011.

[4] A. Böge and W. Böge, *Technische Mechanik: Statik – Reibung – Dynamik – Festigkeitslehre – Fluidmechanik*, 31st ed. Springer Fachmedien Wiesbaden, 2021.

[5] F. Natterer and E. L. Ritman, "Past and future directions in x-ray computed tomography," *International Journal of Imaging Systems and Technology*, vol. 12, no. 4, 2002.

[6] R. Hynd, *The density of meissner polyhedra*, Apr. 8, 2023.

[7] I. Arelio, L. Montejano, and D. Oliveros, "Peabodies of constant width," *Beiträge zur Algebra und Geometrie / Contributions to Algebra and Geometry*, 2022.

[8] Á. G. Horváth, "On convex bodies that are characterizable by volume function," *Arnold Mathematical Journal*, vol. 6, no. 1, 2020.

[9] D. Meschede, *Gerthsen Physik*, 25th ed. Springer Spektrum, 2015.

[10] J. C. Lagarias, Ed., *The Kepler Conjecture: The Hales-Ferguson Proof*, 1st ed. Springer New York, 2011.

[11] W. Jin, P. Lu, and S. Li, "Evolution of the dense packings of spherotetrahedral particles: From ideal tetrahedra to spheres," *Scientific Reports*, vol. 5, no. 1, 2015.

[12] A. Haji-Akbari, M. Engel, A. S. Keys, *et al.*, "Disordered, quasicrystalline and crystalline phases of densely packed tetrahedra," *Nature*, vol. 462, no. 7274, 2009.

[13] M. Jerkins, M. Schröter, H. L. Swinney, T. J. Senden, M. Saadatfar, and T. Aste, "Onset of mechanical stability in random packings of frictional spheres," *Physical Review Letters*, vol. 101, no. 1, 2008.

[14] K. W. Desmond and E. R. Weeks, "Random close packing of disks and spheres in confined geometries," *Physical Review E*, vol. 80, no. 5, 2009.

[15] S. Weis and M. Schröter, "Analyzing x-ray tomographies of granular packings," *Review of Scientific Instruments*, vol. 88, no. 5, 2017.

[16] G. D. Scott and D. M. Kilgour, "The density of random close packing of spheres," *Journal of Physics D: Applied Physics*, vol. 2, no. 6, 1969.

[17] A. Jaoshvili, A. Esakia, M. Porrati, and P. M. Chaikin, "Experiments on the random packing of tetrahedral dice," *Physical Review Letters*, vol. 104, no. 18, 2010.

[18] S. Carmignato, W. Dewulf, and R. Leach, Eds., *Industrial X-Ray Computed Tomography*, 1st ed. Springer International Publishing, 2018.

[19] W. A. Kalender, *Computed tomography: fundamentals, system technology, image quality, applications*, 3rd ed. Publicis Publ, 2011.

[20] H. R. Schwarz and N. Köckler, *Numerische Mathematik*, 8th ed. Vieweg + Teubner, 2011.

[21] N. Otsu, "A threshold selection method from gray-level histograms," *IEEE Transactions on Systems, Man, and Cybernetics*, vol. 9, no. 6, 1979.

[22] W. Silversmith. "Connected components on multilabel 3d images." (2023), [Online]. Available: `https://pypi.org/project/connected-components-3d/` (visited on 05/07/2023).

[23] P. Virtanen, R. Gommers, T. E. Oliphant, *et al.*, "SciPy 1.0: Fundamental Algorithms for Scientific Computing in Python," *Nature Methods*, vol. 17, 2020.

[24] E. Bach, W. Bierwerth, H. H. Herr, and F. Wieneke, *Formeln der Technik: Elektrotechnik, Maschinenbautechnik, Chemietechnik, Mathematik/Physik*, 4th ed. Verlag Europa-Lehrmittel Nourney, Vollmer GmbH & Co. KG, 2017.

[25] H. S. M. Coxeter, *Regular Polytopes*, 3rd ed. Dover Publications, 2012.

[26] M. Neudecker, S. Ulrich, S. Herminghaus, and M. Schröter, "Jammed frictional tetrahedra are hyperstatic," *Physical Review Letters*, vol. 111, no. 2, 2013.